Journal of Alloys and Compounds 509 (2011) 5152–5158

Contents lists available at ScienceDirect

Journal of Alloys and Compounds

journal homepage: www.elsevier.com/locate/jallcom

Synthesis and photoactivity of the highly efficient Ag species/TiO_2 nanoflakes photocatalysts

Yong Liu, Juncheng Hu*, Jinlin Li

Key Laboratory of Catalysis and Materials Science of the State Ethnic Affairs Commission & Ministry of Education, South-Central University for Nationalities, Wuhan 430074, PR China

ARTICLE INFO

Article history:
Received 1 October 2010
Received in revised form 29 January 2011
Accepted 1 February 2011
Available online 1 March 2011

Keywords:
Silver species
Titania nanoflakes
Photodegradation
Dye
Synergy effect

ABSTRACT

Ag species/TiO_2 nanoflakes photocatalysts with different relative contents (Ag^+, Ag^{2+}, Ag^0) have been successfully synthesized by a simple template-free synthetic strategy. X-ray photoelectron spectroscopy, X-ray diffraction, and UV–vis diffuse reflectance spectra indicated that the dopant ions (Ag^+ or Ag^{2+}) were partly incorporated into the titanium dioxide nanoflakes. Meanwhile, part of the silver ions migrated to the surface after the subsequent calcination and aggregated into ultra-small metallic Ag nanoclusters (NCs) (1–2 nm), which are well dispersed on the surface of TiO_2 nanoflakes. The photocatalytic activities of the Ag species/TiO_2 materials obtained were evaluated by testing the photodegradation of the azo dye reactive brilliant X-3B (X-3B) under near UV irradiation. Interestingly, it was found that the maximum photocatalytic efficiency was observed when Ag species coexisted in three valence states (Ag^+, Ag^{2+}, Ag^0 NCs), which was higher than that of Degussa P25. The high photocatalytic activity of the Ag species/TiO_2 can be attributed to the synergy effect of the three Ag species.

1. Introduction

In recent years, flake-like metal oxide nanomaterials have shown excellent catalytic performance for a variety of reactions because of their unique surface chemistry [1–4]. Especially, TiO_2 is one of the most studied semiconductors for environmental cleanup applications [5–10]. However, the low quantum efficiency and high band gap of TiO_2 limit its photocatalytic activity and practical application [11]. So far, many efforts have been frequently employed to further improve the photocatalytic activity of TiO_2 [12–16]. An extensive literature has already described the doping or loading procedure of TiO_2 with noble metal nanoparticles that directly influences the intrinsic properties of TiO_2 and extends its photoresponse into the visible domain [17,18]. In particular, the deposition of silver on TiO_2 has been of considerable interest for both mechanism studies [19] and applications [20–22] as electron traps aiding electron–hole separation. However, little attention was focused on the valence state of the doped metal, and their structure/composition is ill defined in recent works.

A question that arises is which species plays the main catalytic role in the photocatalytic process: metals, metal ions or synergy effect in-between? Recently, Awazu et al. [23] reported a plasmonic photocatalyst which was fabricated by depositing a silver core covered with silica (SiO_2) shell on the surface of TiO_2, the silica shell was used to prevent oxidation of Ag by direct contact with TiO_2, and the photocatalytic activity of such a plasmonic photocatalyst was greatly enhanced under near UV illumination. However, Xin et al. [24] and Falaras et al. [21] reported that Ag^+ doping can not only promote the phase transformation of TiO_2, but also efficiently separate the electron–hole pairs resulting in a much higher photocatalytic activity. Up to now, the knowledge about the functions of noble metal species supported on semiconductors as highly efficient photocatalysts is rather controversial and limited.

Recently, we have reported a simple template-free synthetic strategy to prepare highly efficient and ultrastable Au/TiO_2 photocatalyst [25]. Here, we prepared silver species/TiO_2 nanoflakes catalyst via a consecutive ion adsorption, photoreduction and calcination treatment. For the catalyst, the size and the relative amount of Ag species (Ag^+, Ag^{2+}, Ag^0 NCs) can be well tuned by simply controlling the time of calcinations. More interestingly, we found that the maximum photocatalytic efficiency was observed when Ag species coexisted in three valence states (Ag^+, Ag^{2+}, Ag^0 NCs). To the best of our knowledge, this is the first report on the controllable preparation of the size and the relative amount of Ag species, the synergy effect between the Ag species (Ag^+, Ag^{2+}, Ag^0 NCs) and their relationship with the photocatalytic activity of Ag species/TiO_2 nanoflakes. This work may provide new insights and understanding on the mechanism of photoactivity enhancement for noble metal supported semiconductor catalysts.

* Corresponding author. Tel.: +86 27 67842752; fax: +86 27 67841302.
E-mail address: junchenghuhu@hotmail.com (J. Hu).

0925-8388/$ – see front matter © 2011 Elsevier B.V. All rights reserved.
doi:10.1016/j.jallcom.2011.02.020

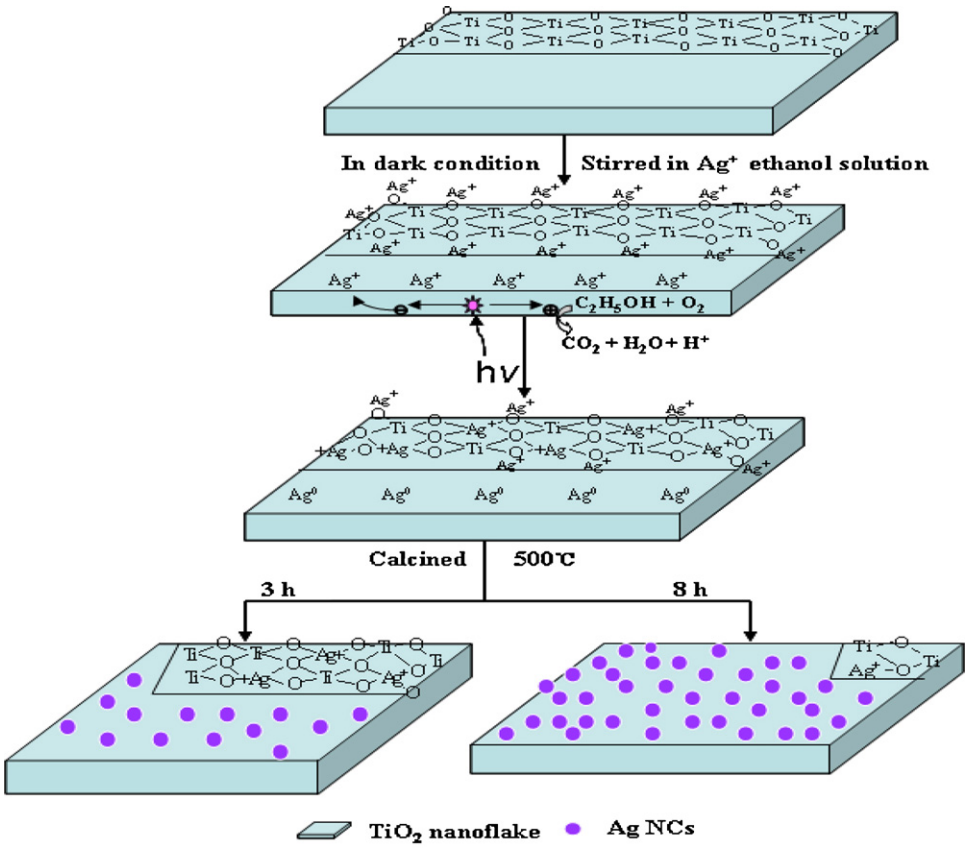

Scheme 1. Graphical representation of the preparation processes for Ag species/TiO_2 catalysts.

2. Experimental

2.1. Preparation of Ag species/TiO_2 photocatalysts

High surface area TiO_2 nanoflakes (BET surface area, 198.3 m^2/g) was purchased from Nanoactive Corporation. The Ag species/TiO_2 catalysts were prepared by a three-step approach (ion adsorption, optical irradiation and finally calcination treatments). In a typical synthesis, 1 g TiO_2 nanoflakes was suspended in 50 ml ethanol solution with 31.5 mg silver nitrate (99.8%, Tianjin Kermel Chemical Agent Company) in a 50 ml glass beaker which was covered by a piece of dark paper. The solution was stirred for 3 h in the dark conditions to facilitate the absorption of silver ion on the surface of TiO_2 nanoflakes. Then, a 300 W high pressure mercury lamp (main-wavelength 365 nm, Shanghai Yaming lighting company) was used for illuminating the suspending solution with magnetic stirring for 3 h. The produced catalyst was filtered and washed with deionized water for 4 times, then washed with ethanol for 3 times and then dried at 80 °C for 20 h. Afterwards, the obtained sample was calcined at 500 °C for 3 h and 8 h in air using a heating rate of 0.5 °C/min, respectively, then the gray Ag species/TiO_2 samples are obtained. The preparation processes are also shown in Scheme 1.

2.2. Characterization of the photocatalyst

The crystalline structure of the catalysts was characterized by Powder X-ray diffraction (XRD) employing a scanning rate of 0.05°/s in a 2θ range from 10° to 80°, in a Bruker D8 Advance using monochromatized Cu Kα radiation. The morphology and particle size of catalysts were analyzed by the transmission electron microscope (TEM), which were taken on a Tecnai G20 (FEI Co., Holland) transmission electron microscope using an accelerating voltage of 200 kV. X-ray photoelectron spectroscopy (XPS) was recorded on a VG Multilab 2000 (VG Inc.) photoelectron spectrometer by using monochromatic Al Kα radiation under vacuum at 2×10^{-6} Pa. All the binding energies were referenced to the C1s peak at 284.8 eV of the surface adventitious carbon. The UV–vis DRS spectra were collected using a Shimadzu UV-2450 spectrophotometer from 200 to 800 nm using $BaSO_4$ as reference. The Surface area was measured using a Micrometrics ASAP 2010 apparatus.

2.3. Photodegradation experiment

The photoactivity of the as-prepared sample was tested by the degradation of reactive brilliant X-3B under near UV irradiation. In a typical experiment, 50 mg photocatalyst and 50 ml aqueous solution of X-3B (1.14×10^{-4} mol/l) were added into a flask, and then the mixed solution was oscillated in darkness overnight. After reaching adsorption equilibrium, the photocatalytic reaction was initiated by irradiating the system with a 300 W Mercury lamp. At given time intervals, 4 ml aliquots were collected, centrifuged, and then filtered to remove the catalyst particles for analysis. The filtrates were finally analyzed by a UV–vis spectrophotometer (UV-2450).

In order to determine the catalyst durability, the photocatalyst was separated from aqueous solution after each run of reactions. The filtered catalyst was reused without any treatment in the subsequent recycling experiment.

3. Results and discussion

3.1. XPS analysis

To investigate both the valence state and the relative amount of different Ag species in the samples, X-ray photoelectron spectroscopy (XPS) experiments were performed. Fig. 1 shows the XPS spectra of O1s region for the as-prepared four samples, which are fitted with the nonlinear least-squares fit program using Gauss–Lorentzian peak shapes. As shown in Fig. 1a, the O1s spectrum of the raw TiO_2 nanoflakes can be fitted into two peaks, which can be assigned to lattice oxygen (529.8 eV, O–Ti) and surface hydroxyl oxygen (531.7 eV, O–H), respectively [26–28]. However, in addition to O–Ti (530.0 eV) and O–H (531.6 eV), the binding energy of 532.6 eV appears for Ag ions/TiO_2, which is attributed to O–Ag^+ resulting from the Ag^+ in the TiO_2 lattice. More interestingly, the O1s region of Ag species/TiO_2 (500 °C, 3 h) is more asymmetric with an obvious shoulder peak, which can be fitted into four peaks corresponding to O–Ti (529.9 eV), O–H (531.6 eV), O–Ag^+ (532.6 eV) and O–Ag^{2+} (533.9 eV), indicating the Ag species coexisted as the three components (Ag^+, Ag^{2+}, Ag NCs) with relative amounts (at%) in the TiO_2 nanoflakes (see Table 1). With the extension of the calcination time to 8 h, Ag^+ ions migrated from the substituted lattice position, to reunite into Ag NCs, so the peak of the O–Ag^+ disap-

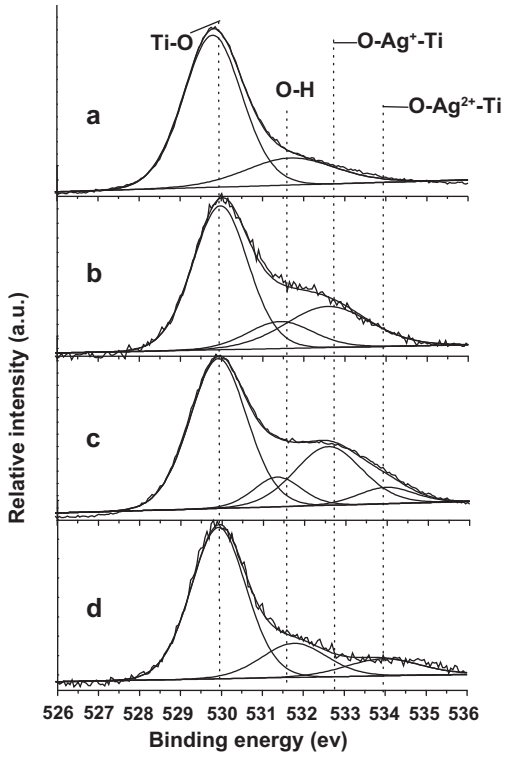

Fig. 1. The XPS spectra of O1s in (a) TiO_2 nanoflakes, (b) Ag ion/TiO_2 nanoflakes, (c) Ag species/TiO_2 nanoflakes (calcined at 500 °C for 3 h), (d) Ag species/TiO_2 nanoflakes (calcined at 500 °C for 8 h).

peared in Fig. 1d. The detailed results of curve-fitting for O1s region is listed in Table 1.

The XPS spectra of $Ag3d_{5/2}$ showed the valence state of Ag species in TiO_2. As seen in Fig. 2a, the three fitted peaks are attributed to Ag^{2+} (366.8 eV), Ag^+ (367.1 eV) and Ag^0 NCs (368.5 eV), respectively [24,29], once again proved that Ag species coexist as Ag^+, Ag^{2+}, Ag^0 NCs in Ag species/TiO_2 (500 °C, 3 h). Meanwhile, the determined binding energies of $Ag3d_{5/2}$ (367.8 eV) and $Ag3d_{3/2}$ (373.8 eV) in Fig. 2b are the characteristic of metallic silver [30], indicating the main silver species existing in TiO_2 (500 °C, 8 h) is

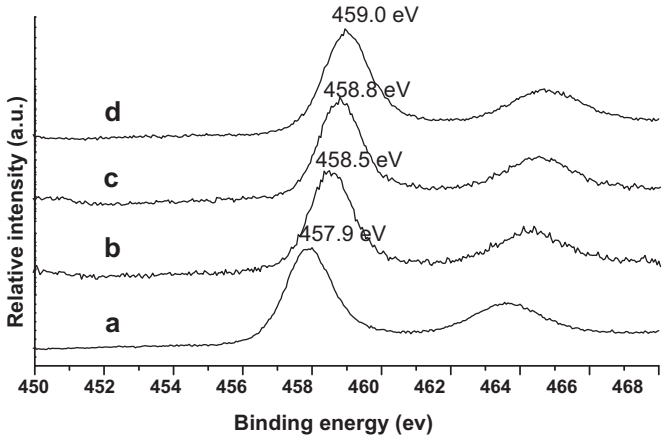

Fig. 3. The XPS spectra of Ti 2p in (a) TiO_2 nanoflakes, (b) Ag ion/TiO_2 nanoflakes, (c) Ag species/TiO_2 nanoflakes (calcined at 500 °C for 8 h), (d) Ag species/TiO_2 nanoflakes (calcined at 500 °C for 3 h).

metallic Ag^0 NCs. The above XPS result of $Ag3d_{5/2}$ is well consistent with the results of O1s in Fig. 1. Moreover, we found that the binding energy of $Ti2p_{3/2}$ in Ag species/TiO_2 slightly shifted from 457.9 to 458.8, 458.9 and 458.7 eV, compared to the pure TiO_2 flakes, respectively (Fig. 3). This approximate 1 eV positive shift can be attributed to the Fermi level of Ag being lower than that of TiO_2. So the conduction band electron of TiO_2 may transfer to the Ag species, resulting in a decrease in the outer electron cloud density of Ti ions [24].

Herein, we proposed a plausible formation mechanism of Ag species/TiO_2 photocatalysts on the basis of TEM observation and XPS analysis. The formation mechanism is shown in Scheme 1: Firstly, the Ag^+ ions were adsorbed strongly on the surface of hydroxylated TiO_2 nanoflakes during the stirring of ethanol solution in the dark condition. However, part of Ag^+ ions was reduced to Ag atoms after the irradiation of UV light for 3 h. Meanwhile, considerable Ag^+ ions incorporated into the TiO_2 lattice. The subsequent calcination treatment (500 °C) promoted the aggregation of Ag^+ ions and Ag atoms into Ag^0 NCs. After the further calcination (8 h), the Ag^+ ions migrated from the substituted lattice position, to aggregate into more Ag^0 NCs.

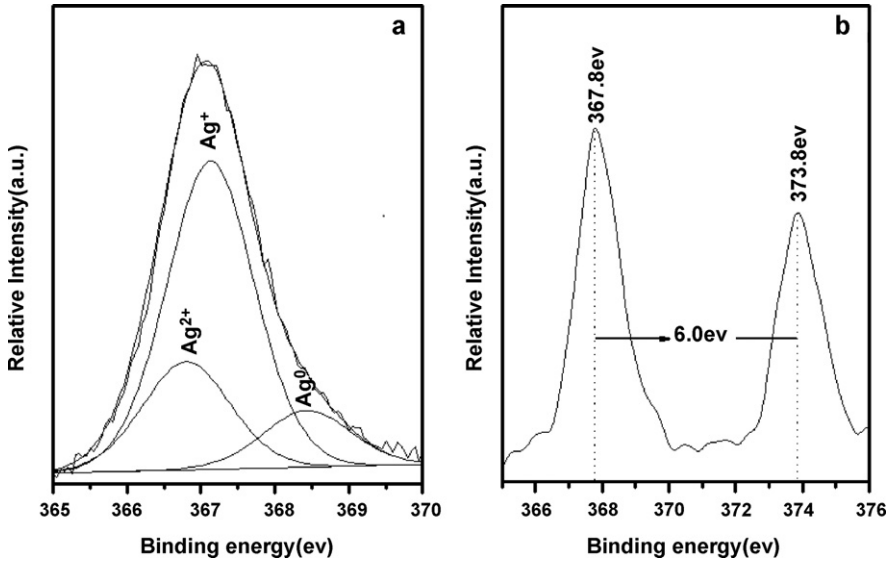

Fig. 2. The XPS spectra of (a) $Ag3d_{5/2}$ of Ag species/TiO_2 (calcined at 500 °C for 3 h), (b) $Ag3d_{3/2}$ and $Ag3d_{5/2}$ of Ag species/TiO_2 (calcined at 500 °C for 8 h).

Table 1
Results of curve-fitting of the XPS spectra for the O1s region of the four samples.

Sample	O1s (O–Ti)	O1s (O–H)	O1s (O–Ag^{+})	O1s (O–Ag^{2+})
TiO_2 (nanoflakes)				
Eb (ev)	529.8	531.7	–	–
at%	78.7	21.3	–	–
Ag ions/TiO_2				
Eb (ev)	530.0	531.6	532.6	–
at%	63.3	12.8	23.9	–
Ag species/TiO_2 (500 °C, 3 h)				
Eb (ev)	529.9	531.6	532.6	534.0
at%	57.8	9.5	26.5	6.2
Ag species/TiO_2 (500 °C, 8 h)				
Eb (ev)	529.9	531.7	–	533.9
at%	70.5	18.8	–	10.7

3.2. TEM analysis

Fig. 4 shows the TEM images of the samples. As shown in Fig. 4a, the pure TiO_2 matrix displayed a flake-like morphology with a crystal size of 20–50 nm. After stirring for 3 h in $AgNO_3$ solution and subsequent UV irradiation for 3 h, we did not observe Ag particles on the surface of TiO_2 in Fig. 4b, indicating that silver ions (Ag^{+}) are anchored strongly on the surface of TiO_2 nanoflakes and part of Ag^{+} incorporated into the TiO_2 lattice. However, as seen in Fig. 4c and d, homogenously dispersed Ag nanoclusters (1–2 nm) on the surface of nanoflakes were observed after the calcination at 500 °C for 3 h and 8 h, respectively. To the best of our knowledge, such uniform dispersion of ultrafine metal nanoclusters onto the entire region of TiO_2 support without using any template or capping agent was realized for the first time. It is worth noting that the number of Ag nanoclusters (NCs) increased obviously with the extension of calcination time from 3 h to 8 h, indicating that the calcination treatment promoted the aggregation of silver ions and atoms into more Ag NCs.

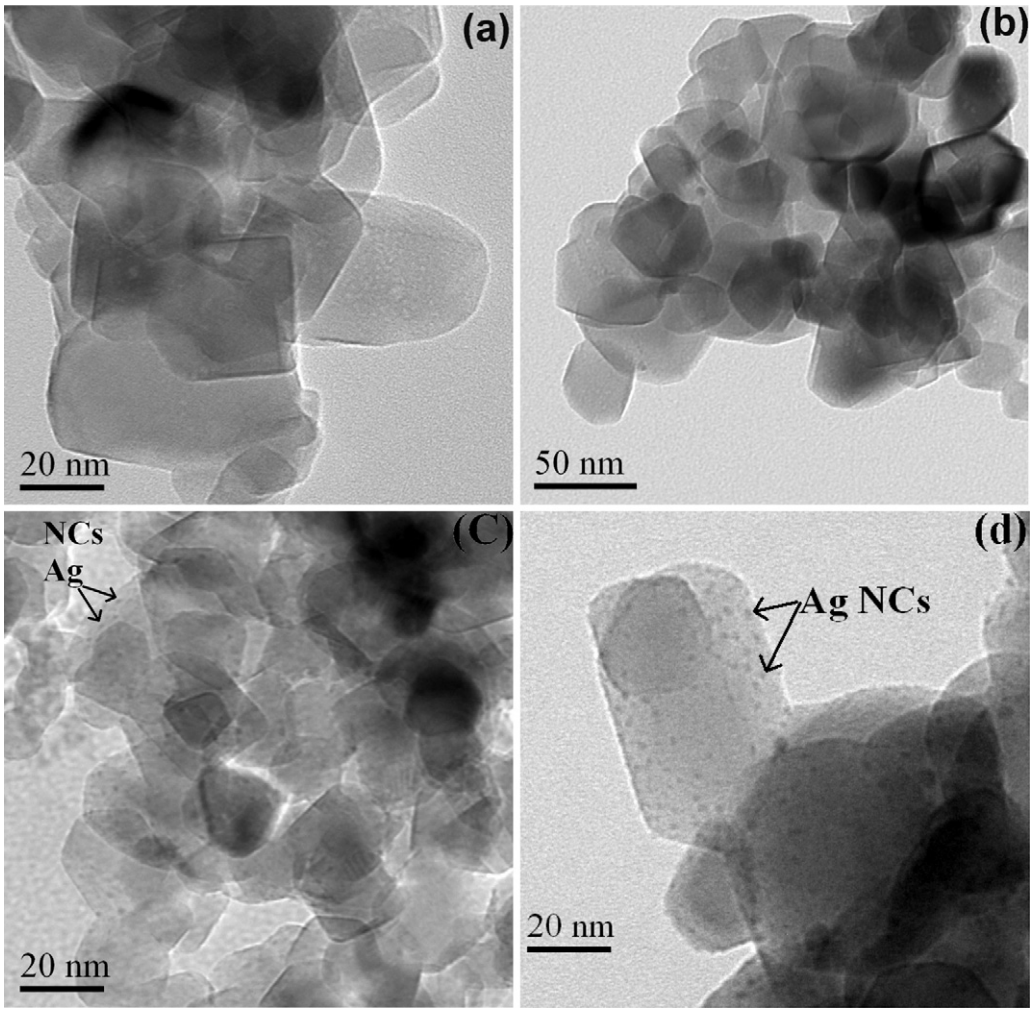

Fig. 4. TEM images of (a) TiO_2 nanoflakes, (b) Ag ion/TiO_2 nanoflakes, (c) Ag species/TiO_2 nanoflakes (calcined at 500 °C for 3 h), (d) Ag species/TiO_2 nanoflakes (calcined at 500 °C for 8 h).

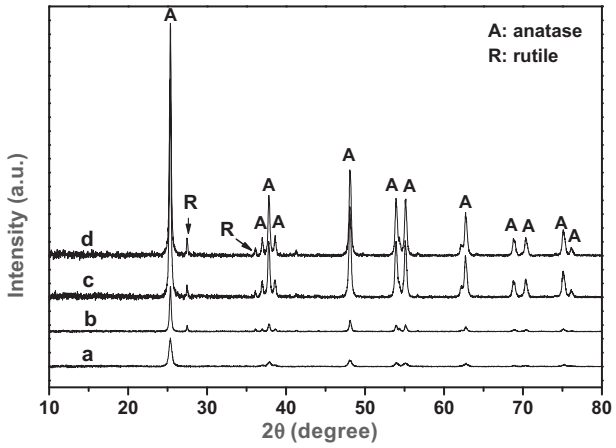

Fig. 5. The XRD patterns of (a) TiO_2 nanoflakes, (b) Ag ion/TiO_2 nanoflakes, (c) Ag species/TiO_2 nanoflakes (calcined at 500 °C for 3 h), (d) Ag species/TiO_2 nanoflakes (calcined at 500 °C for 8 h).

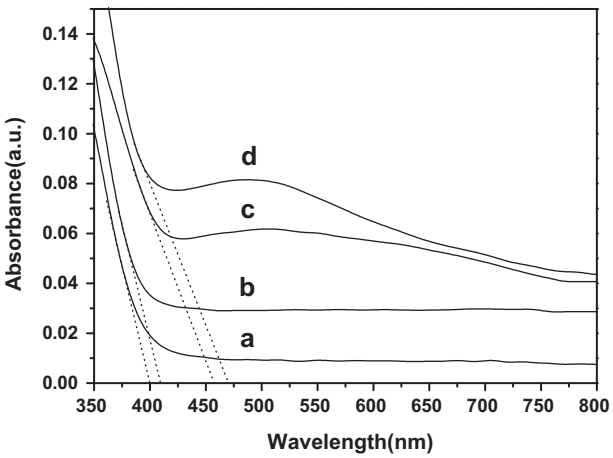

Fig. 6. UV–visible diffuse reflectance spectra of (a) TiO_2 nanoflakes, (b) Ag ion/TiO_2 nanoflakes, (c) Ag species/TiO_2 nanoflakes (calcined at 500 °C for 8 h), (d) Ag species/TiO_2 nanoflakes (calcined at 500 °C for 3 h).

3.3. XRD analysis

Fig. 5 shows the XRD patterns of the four samples. It is obvious that pure TiO_2 was in pure anatase phase (JCPDS No. 01-086-1156), no characteristic peaks of other phases such as rutile and brookite were observed. However, we observed the following two significant changes when compared to the pure TiO_2 nanoflakes: (a) The characteristic diffraction peaks of (1 1 0) and (1 0 1) planes corresponding to rutile emerges apparently, indicating that doping Ag species can assist the phase transformation, which is in accordance with the observation of Xin et al. [24]. As Xin et al. suggested, there are two possible reasons for the phase transformation. One was that the density of surface defects of TiO_2 would increase with Ag doping, which would promote the phase transformation because the surface defects were considered as the rutile nucleation sites [31]. Another was that the surface oxygen vacancy concentration of anatase grains increased with Ag doping [32], which favored the rearrangement of ions and re-organization of structure for rutile phase. (b) We observed a slight shift in the TiO_2 (1 0 1) to lower 2θ values with doping Ag species (see Table S1), which corresponded to the increase of d spacing. This observation could be attributed to the incorporation of Ag^+ into the TiO_2 lattice. However, no obvious diffraction peaks of Ag are found, which can be attributed the following two aspects: one is the low doping concentration of Ag (2 wt%), the other is that some of the doped Ag is present as ions in TiO_2 matrix lattice.

3.4. DRS analysis

The optical absorption properties of the samples were investigated by UV–vis diffuse reflectance spectra (DRS). From Fig. 6, it can be seen the absorption intensity of the Ag species/TiO_2 samples increased greatly in all detected wavelength range, compared to pure TiO_2 nanoflakes. This property is very important for phtocatalysts, the enhanced light absorption indicates the catalysts can provide more photocharges for the photocatalytic reactions. It is clear that the strong absorption occurs in the visible light region (400–650 nm) for Ag species/TiO_2 (500 °C, 3 h). The origin of this visible light absorption is due to the formation of a dopant energy level within the band gap of TiO_2 [33], implying that doping Ag species changed the band gap of TiO_2 matrix. Herein, the band gap energies estimated from the intercept of the tangents to the plots were found to be 3.2 eV, 3.1 eV, 2.7 eV and 2.6 eV for pure TiO_2 nanoflakes, Ag ions/TiO_2, Ag species/TiO_2 (500 °C, 8 h) and Ag species/TiO_2 (500 °C, 3 h), respectively.

3.5. BET analysis

The specific surface areas and pore sizes of Ag species/TiO_2 catalysts were measured. The results are presented in Fig. S1. According to the BDDT classification, the isotherm obtained is of type IV with two capillary condensation steps. The pore size distributions were shown in Fig. S2. The corresponding BET surface areas of TiO_2 nanoflakes, Ag species/TiO_2 (500 °C, 3 h) and Ag species/TiO_2 (500 °C, 8 h) were determined as 198.3, 7.40 and 4.60 m^2/g, respectively. Selected properties of the samples are summarized in Table S3.

3.6. Photocatalytic activity

To evaluate the photocatalytic capability of the samples, we examined the photodegradation of brilliant red X-3B azo dye solution under near UV irradiation (365 nm). X-3B dye is a chemically stable and poorly biodegradable dye contaminant in wastewater, its characteristic absorption at λ = 535 nm was used to monitor the photocatalytic degradation process. The installation of the photoreactor is shown in Fig. S3 (see the Supporting Information). When the reactions were conducted without catalyst, no reactions were observed even after 3 h (Fig. 7f). For comparison, we also

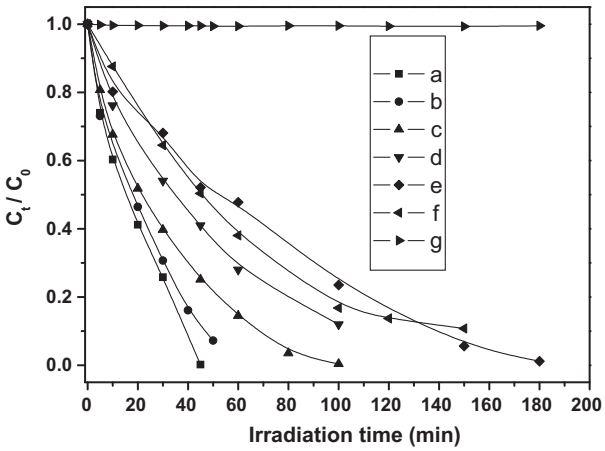

Fig. 7. c_t/c_0 vs time curves of X-3B photodegradation over the samples: (a) Ag species/TiO_2 nanoflakes (calcined at 500 °C for 3 h), (b) Degussa P25 TiO_2, (c) Ag species/TiO_2 nanoflakes (calcined at 500 °C for 8 h), (d) Ag species/Degussa P25, (e) Ag ion/TiO_2 nanoflakes, (f) TiO_2 nanoflakes, (g) without photocatalyst.

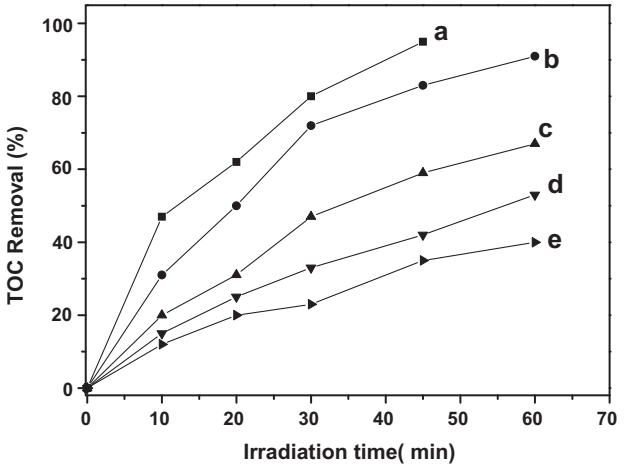

Fig. 8. Removal percentage of TOC in the photocatalytic degradation of X-3B solution over the five samples: (a) Ag species/TiO_2 nanoflakes (calcined at 500 °C for 3 h), (b) Degussa P25 TiO_2, (c) Ag species/TiO_2 nanoflakes (calcined at 500 °C for 8 h), (d) Ag ion/TiO_2 nanoflakes, (e) TiO_2 nanoflakes.

carried out the decomposition of the X-3B in solution over the Degussa P25 TiO_2. As shown in Fig. 7, the pure TiO_2 nanoplakes exhibited low activity due to its large energy gap (3.2 eV). However, the decomposition of X-3B over the Ag specie/TiO_2 (500 °C, 3 h) catalyst completed quickly only in 45 min. Meanwhile, the photocatalytic efficiency was in the following order: Ag species/TiO_2 (500 °C, 3 h) > Degussa P25 > Ag species/Degussa P25 (500 °C, 3 h) > Ag species/TiO_2 (500 °C, 8 h) > Ag ions/TiO_2 ≈ TiO_2 nanoflakes, indicating that the doping of silver species can greatly improve the photocatalytic activity of matrix TiO_2 nanoflakes. Especially, the maximum photocatalytic efficiency was observed when silver species existed together with the three oxidation states (Ag^+, Ag^{2+}, Ag^0 NCs), which was even higher than that of Degussa P25. The total organic carbon (TOC) disappearance for the organic molecules (X-3B) is represented in Fig. 8 as a function of irradiation time. The values of percentage degradation and TOC removal confirm that degradation and mineralization are well pronounced in the presence of catalyst. Fig. 9 shows the change of absorption spectra of an X-3B aqueous solution in the presence of Ag specie/TiO_2 (500 °C, 3 h) catalyst under UV light irradiation.

The linear relationships of $\ln(c_0/c_t)$ versus time revealed that the photodegradation reaction followed a pseudo-first-order reactions. The apparent first-order reaction rate constants for the cases of Ag

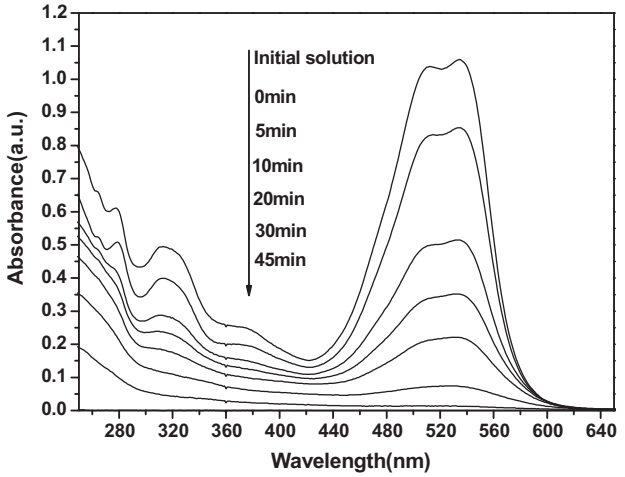

Fig. 9. Absorption spectrum of a solution of X-3B (1.14×10^{-4} M, 50 ml) in the presence of Ag specie/TiO_2 (500 °C, 3 h, 50 mg) under UV light irradiation.

Table 2
The kinetic constants, regression coefficients and the kinetics equation and for the photodegradation of X-3B by the five samples.

Samples	k (min^{-1})	R^2	The kinetics equation
Ag species/TiO_2 (500 °C, 3 h)	0.0740	0.9784	$y = 0.074x - 0.4243$
Degussa P25	0.0607	0.9753	$y = 0.0607x + 0.0421$
Ag species/TiO_2 (500 °C, 8 h)	0.0506	0.9239	$y = 0.0506x - 0.4243$
Ag species/Degussa P25 (500 °C, 3 h)	0.0208	0.9964	$y = 0.0208x + 0.0129$
Ag ions/TiO_2	0.0175	0.9575	$y = 0.0175x - 0.1042$
TiO_2 (nanoflakes)	0.0161	0.9871	$y = 0.0161x - 0.0114$

species/TiO_2 (500 °C, 3 h), Ag species/TiO_2 (500 °C, 8 h), Ag ions/TiO_2 and TiO_2 nanoflakes were 0.074, 0.0506, 0.0175 and 0.0161 min^{-1} (Table 2), respectively, indicating the photodegradation rate of Ag species/TiO_2 (500 °C, 3 h) was 4.6 times higher than that of pure TiO_2 nanoflakes. It is well known that the photocorrosion or photodissolution of catalyst often occurs on the photocatalyst surface in the photocatalytic reaction. Herein, to test the repeatability of X-3B dyes photodegradation on Ag species/TiO_2 (500 °C, 3 h), we carried out the phodegradation experiments repeatedly for seven times. As shown in Fig. S4 in the Supporting Information, the X-3B dye is quickly degraded after every injection of the X-3B solution, indicating the photocatalyst Ag species/TiO_2 (500 °C, 3 h) is stable under repeated application with nearly constant photodegradation rate.

3.7. Photocatalytic mechanism

In our case, for the Ag ions/TiO_2 and pure TiO_2 nanoflakes photocatalysts, the Ag ions doping can actually promote the phase transformation from anatase to rutile (see Fig. 5a and b), however, little improvement of photocatalytic activity was observed with phase transition of TiO_2 (comparing Fig. 7d and e). Meanwhile, for the Ag species/TiO_2 (500 °C, 3 h) and Ag species/TiO_2 (500 °C, 8 h) photocatalysts, they have nearly the same weight ratios of anatase and rutile phases (see Table S2), but very different photocatalytic efficiencies was found due to their different relative amounts of Ag species in TiO_2 matrix (comparing Fig. 7a and c). According to the above result of the photodegradation and the morphology, structure and composition analysis, we believe that the enhanced photocatalytic activity can be attributed to the Ag species in TiO_2 matrix, rather than the phase transformation or BET surface area (see comparison data in Table S3). Then, how to understand the degradation mechanism of Ag species/TiO_2 catalysts?

It is well known that the lifetime of photogenerated charges (electron and hole) is critical for the effective degradation reaction, charge-trapping in the transition-metal is conductive to separation of the photogenerated electron–hole pairs, which leads to an enhancement of the photocatalytic activity of TiO_2 matrix. From the results of XPS, we found that Ag species coexist in three oxidation state (Ag^+, Ag^{2+}, Ag^0 NCs) in Ag species/TiO_2 (500 °C, 3 h), and their synergy effect in separating the photogenerated electron–hole pairs here is considered to play the main role in improving the photocatalytic activity (see Scheme 2). First, since the Ag^0 NCs Fermi level is lower than that of TiO_2, the photogenerated electrons can transfer to the Ag particles deposited on the surface of TiO_2 nanoflakes, resulting in the effective separation of the electrons–hole pairs and then migrated to O_2 to generate O_2^-. In the meantime, Ag^+ can also serve as a hole trap: $Ag^+ + h^+ \rightarrow Ag^{2+}$. In contrast to the community (Ag^+, Ag^{2+}, Ag^0 NCs), which can act as both electron and hole traps, the single specie Ag^+(Ag^{2+}) or Ag^0 NCs can act as hole or electron trap. This explains why Ag specie/TiO_2

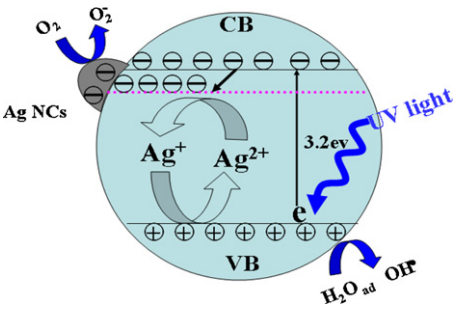

Scheme 2. The graphical representation of the mechanism for improving the photocatalytic activity over Ag species/TiO_2 nanoflakes photocatalysts.

(500 °C, 3 h) shows much higher photocatalytic activity than Ag ions/TiO_2 and Ag species/TiO_2 (500 °C, 8 h).

4. Conclusions

This work demonstrated a novel and simple synthetic strategy for preparing high-efficiency and stable Ag species/TiO_2 nanoflakes catalyst. For the catalyst, the variety and relative amount of Ag species in TiO_2 matrix can be well tuned by controlling the time of calcinations. We believe that the synergy effect of Ag species in separating the photogenerated electron–hole pairs is the key factor for improving the photocatalytic activity of TiO_2 nanoflakes. Our work also provided new insights and understanding on the mechanism for the photoactivity enhancement of the nobel metal supported semiconductor catalysts.

Acknowledgements

The project was sponsored by the Scientific Research Foundation for the Returned Overseas Chinese Scholars, State Education Ministry. This work was also supported by National Natural Science Foundation of China (20803096), Department of Science and Technology of Hubei Province (2010CDA082) and South-Central University for Nationalities (YZZ 08002).

Appendix A. Supplementary data

Supplementary data associated with this article can be found, in the online version, at doi:10.1016/j.jallcom.2011.02.020.

References

[1] X.G. Han, Q. Kuang, M.S. Jin, Z.X. Xie, L.S. Zheng, J. Am. Chem. Soc. 131 (2009) 3152–3153.
[2] J.C. Hu, K.K. Zhu, L.F. Chen, C. Kuebel, R. Richards, J. Phys. Chem. C 111 (2007) 12038–12044.
[3] H.G. Yang, G. Liu, S.Z. Qiao, C.H. Sun, S.C. Smith, H.M. Cheng, J. Zou, G.Q. Lu, J. Am. Chem. Soc. 131 (2009) 4078–4083.
[4] J.C. Hu, K.K. Zhu, L.F. Chen, H.J. Yang, Z. Li, A. Suchopar, R. Richards, Adv. Mater. 20 (2008) 267–271.
[5] A. Fujishima, K. Honda, Nature 238 (1972) 37–38.
[6] B. O'Regan, M. Gratel, Nature 353 (1991) 737–740.
[7] R. Cai, Y. Kubota, T. Shuin, H. Saikai, K. Hashimoto, A. Fujishima, Cancer Res. 52 (1992) 2346–2348.
[8] D. Guin, S.V. Manorama, J.N.L. Latha, S. Singh, J. Phys. Chem. C 111 (2007) 13393–13397.
[9] A. Mills, S. Le Hunte, J. Photochem. Photobiol. A: Chem. 108 (1997) 1–36.
[10] M.R. Hoffman, S.T. Martin, W.D. Choi, W. Bahnemann, Chem. Rev. 95 (1995) 69–96.
[11] R. Asahi, T. Morikawa, T. Ohwaki, K. Aoki, Y. Taga, Science 293 (2001) 269–271.
[12] X.B. Chen, L. Liu, P.Y. Yu, S.S. Mao, Science (2011), doi:10.1126/science.1200448.
[13] M. Salari, S.M. Mousavi khoie, P. Marashi, M. Rezaee, J. Alloys Compd. 469 (2009) 386–390.
[14] H. Yang, C.X. Pan, J. Alloys Compd. 501 (2010) L8–L11.
[15] I. Stambolova, V. Blaskov, S. Vassilev, M. Shipochka, C. Dushkin, J. Alloys Compd. 489 (2010) 257–261.
[16] R.M. Mohamed, I.A. Mkhalid, J. Alloys Compd. 501 (2010) 143–147.
[17] J.X. Sun, G. Chen, Y.X. Li, C. Zhou, H.J. Zhang, J. Alloys Compd. 469 (2011) 1133–1137.
[18] L. Baia, L. Diamandescu, L. Barbu-Tudoran, A. Peter, G. Melinte, V. Danciu, M. Baia, J. Alloys Compd. 509 (2011) 2672–2678.
[19] J. He, I. Ichinose, T. Kunitake, A. Nakao, Langmuir 18 (2002) 10005–10010.
[20] C. He, Y. Xiong, J. Chen, C.H. Zha, X.H. Zhu, J. Photochem. Photobiol. A 157 (2003) 71–79.
[21] I.M. Arabatzis, T. Stergiopoulos, M.C. Berbard, D. Labou, S.G. Neophytides, P. Falaras, Appl. Catal. B 42 (2003) 187–201.
[22] E. Szabó-bárdos, H. Czili, A. Horváth, J. Photochem. Photobiol. A 154 (2003) 195–201.
[23] K. Awazu, M. Fujimaki, C. Rockstuhl, J. Tominaga, H. Murakami, Y. Ohki, N. Yoshida, T. Watanable, J. Am. Chem. Soc. 130 (2008) 1676–1680.
[24] B.F. Xin, L.Q. Jing, Z.Y. Ren, B.Q. Wang, H.G. Fu, J. Phys. Chem. B 109 (2005) 2805–2809.
[25] Y. Liu, L.F. Chen, J.C. Hu, J.L. Li, R. Richards, J. Phys. Chem. C 114 (2010) 1641–1645.
[26] J. Li, H.C. Zeng, Chem. Mater. 18 (2006) 4270–4277.
[27] E.L. Bullock, L. Patthey, S.G. Steinemann, Surf. Sci. 352–354 (1996) 504–510.
[28] S.D. Senanayake, H. Idriss, PNAS 103 (2006) 1194–1198.
[29] C.D. Wagner, W.M. Riggs, L.E. Davis, J.F. Moulder, Handbook of X-ray Photoelectron Spectroscopy, Perking-Elmer Corp., Physical Electronics Division, Eden Prairie, MN, 1979.
[30] J.F. Moulder, W.F. Stickle, P.E. Sobol, K.D. Bomben, Handbook of X-ray Photoelectron Spectroscopy, 2nd ed., Perkin-Elmer Corp, Waltham, MA, 1992.
[31] J.M.G. Amores, V.S. Escribano, G. Busca, J. Mater. Chem. 5 (1995) 1245–1249.
[32] H.E. Chao, Y.U. Yun, H.U. Xingfang, A. Larbot, J. Eur. Ceram. Soc. 23 (2003) 1457–1464.
[33] X.H. Wang, J.G. Li, H. Kamiyama, Y. Moriyoshi, T. Ishigaki, J. Phys. Chem. B 110 (2006) 6804–6809.